# Intelligent Rail Transit Research: The Application of Dynamic Distance Measurement in Gauge Detection System

Jiyue Wang[1]

School of Vehicle and Traffic Engineering, Zhengzhou University of Science and Technology
Zhengzhou 450064 China
wangjiyue@163.com
*Received Dec. 25, 2024; Revised and Accepted Jan. 2, 2025*

**Abstract.** Manual operation of gauge calibrator is tedious and time-consuming. The automatic transformation of calibrator is realized through the integration of motion control and machine vision technology. Two closed-loop positioning subsystems are composed of digital caliper length standard, chain drive mechanism and stepping motor to realize automatic motion control of gauge and ultra-high parameter measurement points. According to the luminance, geometric shape structure and fitting feature information, all kinds of indicator features and their relationships are identified in the display dial image to realize machine vision reading. The noise is removed by image difference method, the image is binarized by adaptive iterative threshold method, and the cross section contour of the track is obtained by expansion and thinning algorithm. The experimental results show that this method can effectively realize the high-precision dynamic measurement of gauge parameters.

**Keywords:** Intelligent rail transit, closed-loop positioning subsystem, machine vision, adaptive iterative threshold.

## 1. Introduction

In the maintenance of urban rail transit lines, gauge parameter is an essential inspection item in track inspection. The traditional detection method uses photoelectric sensing and servo mechanism to measure [1]. The main disadvantage of this detection method is that field vibration is easy to cause damage to the servo mechanism. Machine vision can quickly obtain a lot of information and automatically process data, which has been widely used in modern automated production condition monitoring, product inspection and quality control. Using the method based on machine vision to measure gauge parameters can effectively improve the efficiency and accuracy of gauge detection, reduce the detection cost, and contribute to the realization of intelligent track detection [2-4].

With the rapid development of high-speed railway and urban rail transit in our country, the need of track inspection and maintenance is increasing, which is directly related to the safety of train operation. Most of the developed countries abroad use intelligent track inspection systems, such as Switzerland PALAS, the Netherlands BSM, Australia RAILSCAN, etc, but this kind of large automated track inspection car is expensive, and the use affects the scheduling of transportation [5-9]. In the daily maintenance of ordinary railway lines in China, portable gauge gauges that can directly measure the gauge between two rail lines and ultra-high parameters are still widely used, and compulsory verification is carried out based on domestic gauge gauges to ensure their metrology performance in accordance with the requirements of JJG 219-2008 ”Standard gauge Railway gauge Verification Regulations”. At present, the domestic testing institutions involved in railway measurement basically use the gauge gauge calibrators made by Shenyang Railway Bureau Sujiatun gauge gauge factory, Harbin Antong measurement and control and other professional railway measuring equipment manufacturers. This kind of calibrator adopts manual mechanical structure for multi-point positioning and manual reading when measuring the gauge, so the verification process is tedious and time-consuming. Ibrar et al. [10] improved the mechanical structure of the calibrator and improved the ease of operation, but it was still manual detection. Regardless of the literature, the electric control part is added, but it does not have a complete automatic detection function. In this paper, the automatic verification function of the equipment is effectively integrated on the original calibration base by motion control and machine vision technology, and the level and efficiency of the calibration of the gauge are improved.

## 2. Detection Principle Based on Machine Vision Measurement Method

Fan light sources 1 and 2 are installed inside the left and right rail. The fan-shaped light source shining vertically on the rail will form a rail half-section outline on the inside of the rail. The images of rail cross section were

captured by $C_1$, $C_2$, $C_3$ and $C_4$ cameras on both sides of the left and right rail [11-15]. Camera $C_i(i = 1, 2, 3, 4)$ uses CCD (charge-coupled device) cameras. Through image analysis, matching and stereo vision algorithm, the spatial coordinates (gauge points) at 16 mm below the top of the left and right rail are obtained. According to the theory of binocular vision system, assuming that the camera of the left binocular vision system (composed of $C_1$ and $C_2$ cameras) has been calibrated, the internal parameters $A_1$ and $A_2$ of $C_1$ and $C_2$ cameras and the geometric relationship $R_{1,2}$ and $T_{1,2}$ between them can be known. If the world coordinate system of the binocular vision system is fixed on the optical center of the camera $C_1$, their projection matrices are $M_1 = A_1 I = A_1$, $M_2 = A_2[R_{1,2}T_{1,2}]$ is the identity matrix. The projection relationship can be expressed by the following equations (1) and (2):

$$z_{c^1}[u_1, v_1, 1]^{-1} = M_1[x_{wl}, y_{wl}, z_{wl}, 1]^{-1}. \tag{1}$$

$$z_{c^2}[u_2, v_2, 1]^{-1} = M_2[x_{wl}, y_{wl}, z_{wl}, 1]^{-1}. \tag{2}$$

Where $z_{c^1}$ and $z_{c^2}$ are the components of space points in camera coordinates, which can be eliminated during calculation. $(u^1, v^1)$ and $(u^2, v^2)$ are the image coordinates of the track point $p_l$ in the images taken by the camera $C_1$ and $C_2$ respectively, which can be obtained through image analysis and matching [16,17].

Similarly, for the right binocular vision system (composed of $C_3$ and $C_4$ cameras), the space coordinates $(x_{wr}, y_{wr}, xz_{wr})$ of the right rail gauge point $p_r$ can be obtained by fixing the world coordinate system to the optical center of the camera $C_3$. In addition, the geometric relation $R_{1,3}$ and $T_{1,3}$ between camera $C_3$ and $C_1$ can also be obtained by means of calibration, so that the space coordinates $(x_{wl}, y_{wl}, xz_{wl})$, $(x_{wr}, y_{wr}, xz_{wr})$ of $p_l$ and $p_r$ and can be mapped to the same world coordinate system. The distance between $p_l$ and $p_r$ can be calculated by the space distance formula, that is, the required gauge value.

## 3. Calibration

Calibration is concerned with the accuracy and stability of the system inspection. The calibration of the gauge detection system consists of two parts: one is the calibration of a single camera to determine the internal parameters, and the other is the calibration of the gauge system to determine the geometric relationship of the four cameras on the left and right sides.

At present, the classical calibration algorithms for different camera models mainly include linear algorithm (DLT), nonlinear algorithm, two-step algorithm, two-plane method and active calibration method [18,19]. In the nonlinear algorithm, the method of using plane template to calibrate camera and vision system has great influence. The method uses a lattice template with accurate positioning (usually a checkerboard template); The template is fixed on a plane, and the camera takes more than 2 template images in different directions; By matching the points on the template with the image points, the mapping matrix between the image and the template is calculated, and the internal parameters of the camera can be solved linearly through the matrix. This method has high calibration accuracy and is easy to use, especially suitable for engineering site calibration. The gauge detection system based on machine vision is calibrated based on this method.

The internal and external parameters of the four cameras are obtained by single camera calibration method. If the external parameters are represented by $R_i$ and $t_i(i = 1, 2, \cdots, 4)$ respectively, $R_i$ and $t_i$ represent the relative position between the camera $RC_i$ and the world coordinate system. Because the binocular vision system of the left and right rail faces back, the image of the calibration template taken by the camera of the left and right rail is only part of the image at both ends of the template. However, when the world coordinate system is fixed on the template, the relative position of the spatial coordinates of all corner points on the template only has a translation relationship. For any two points $p_l$ and $p_r$ on the template that can be photographed in the left and right binocular vision system, and their relationship in the camera coordinate system, it can be expressed by the following formulas (3-7):

$$X_{c^1} = R_1 X_{wl} + t_1. \tag{3}$$

$$X_{c^2} = R_{12} X_{wl} + t_2. \tag{4}$$

$$X_{c^3} = R_3 X_{wl} + t_3. \tag{5}$$

$$X_{c^4} = R_4 X_{wl} + t_4. \tag{6}$$

$$X_{wl} = X_{wr} + t_{lr}. \tag{7}$$

Where $X_{wl}$, $X_{wr}$ represents the world coordinates of $P_t$ and $P_r$. $t_{lb}$ is the translation relationship between $X_{wl}$ and $X_{wr}$. $X_{ci}(i = 1, 2, 3, 4)$ is the coordinates of the camera $C_i$ coordinate system. Therefore, the obtained geometric relationship between the four cameras is as follows:

$$R_{1,2} = R_1 R_2^{-1}, T_{1,2} = t_1 - R_1 R_2^{-1} t_2. \tag{8}$$

$$R_{1,3} = R_1 R_3^{-1}, T_{1,3} = t_1 - R_1 R_3^{-1} t_3 + t_{lr}. \tag{9}$$

$$R_{2,3} = R_2 R_3^{-1}, T_{2,3} = t_1 - R_2 R_3^{-1} t_3 + t_{lr}. \tag{10}$$

$$R_{3,4} = R_3 R_4^{-1}, T_{3,4} = t_3 - R_4^{-1} t_4. \tag{11}$$

## 4. Image Processing

RGB (red, green and blue) color mode is the most commonly used color space for hardware devices, and most image acquisition devices use CCD technology as the core technology to directly perceive the 3 components of color R, G, B. In the design of gauge detection system, it is considered to use color light with high power to directly collect color images. According to the color of the light source is fixed and single, the image component separation method and the image shadow difference algorithm are used to achieve the noise removal and binarization of the image [20]. The morphological image processing method is used to process the binarization image, and the rail profile is extracted. Finally, the gauge value is obtained by visual algorithm. The image processing flow of the gauge detection system based on machine vision is shown in Figure 1.

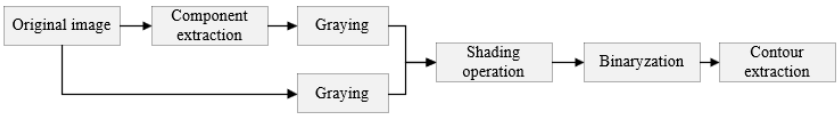


**Fig. 1.** Image processing flow of gauge detection system based on machine vision

### 4.1. Image Segmentation

The gauge detection system based on machine vision uses a red fan-shaped laser light source, and the rail images collected by the camera have obvious red rail half-section profile light strip and rail background. Due to the change of external illumination, it is difficult to segment the target region and background region accurately by histogram combined with threshold value in the actual process of image acquisition. And the image target area is small, which is completely submerged in the background noise in the histogram. However, because the color features of the light band are relatively fixed, the R component in the original rail RGB image can be extracted separately. This method is effective and preserves the rail profile features to the greatest extent.

### 4.2. Image Aberration

The difference image provides the difference information between images, which can be used to guide dynamic detection, moving target detection and tracking, image background elimination and target recognition. Image subtraction can be used to remove unwanted additive patterns in an image. Additive patterns may be slowly changing background shadows, periodic noise, or additional pollution known at every pixel on the image. Its mathematical expression is as follows:

$$C(x, y) = A(x, y) - B(x, y). \tag{12}$$

Where $A(x, y)$ is the current image. $B(x, y)$ is a fixed background image (matching template). $C(x, y)$ is the output image.

The purpose of shading is to eliminate unnecessary image content that is common to both images. The corresponding image points of the two subtracting images must be located on the same target point in space when the image is used for the difference calculation. This algorithm uses the extraction of R component to obtain the image as the current $A(x, y)$, and the grayscale image of the original RGB image as the background image $AB(x, y)$, so the corresponding points of the two images are exactly corresponding, and the additive noise of the image can be effectively eliminated.

### 4.3. Binaryzation

In order to meet the requirement of real-time dynamic image processing, adaptive iterative threshold method is used to binarize gray image. Firstly, an approximate threshold $T$ is selected and the image $C(x, y)$ is divided into two parts. Then the mean values $U1$ and $U2$ are calculated respectively, and a new segmentation threshold $T = (U1 + U2)/2$ is selected. Repeat the above steps until $U1$ and $U2$ are no longer changing. The iterative method is based on the idea of approximation and its steps are as follows:

1. Calculate the maximum and minimum gray values of the image, denoted as $Z_{max}$ and $Z_{min}$ respectively, and make the initial threshold $T_0 = (Z_{max} + Z_{min})$.
2. According to the threshold value $T$, the image is divided into foreground and background, and the average gray values of $Z_O$ and $Z_B$ are obtained respectively.
3. Find the new threshold $T = (Z_O + Z_B)/2$.
4. If the two average gray values $Z_O$ and $Z_B$ do not change (or $T$ does not change), then $T$ is the threshold value, otherwise go to step (2) to continue the iterative calculation.

The image $C(x, y)$ obtained by the difference image operation is segmented by the adaptive threshold to obtain the binary image of the rail section. Using this algorithm, the interference of background noise and track surface bright spot can be completely eliminated.

### 4.4. Contour Feature Extraction

There will be some breakpoints after image binarization, which is not conducive to the effective extraction of rail contour. Therefore, it is necessary to expand the binary image vertically and horizontally according to the contour image features [21-25]. The expansion operators are:

$$V = H = [11111]. \tag{13}$$

The expansion operation satisfies the associative law. The dilatation operation on a binary image is expressed as:

$$C = A \oplus V \oplus H. \tag{14}$$

Where $C$ is image after expansion. $A$ is binary image. $V$ and $H$ are vertical and horizontal expansion operators respectively.

First inflate with column structure elements, then inflate with row structure elements. The decomposition form is 2.5 times faster than the separate expansion of $5 \times 5$ array, and the operation time is saved. The image obtained after expansion is refined. Hilditch refinement algorithm is used in this process. Hilditch refinement algorithm is an effective binary image refinement algorithm. Its main idea is to delete the contour pixels of the target in the image every scan until no contour pixels can be deleted in the image, and finally obtain a rail section contour line with a pixel width.

## 5. Experimental Analysis

A German AVT CCD camera with a pixel resolution of one $280 \times 960$ is used in the test, and the industrial computer is connected through PCI bus 1394B board, and a red sector light source with an output wavelength of 635nm is used to form a gauge detection system. The rail is placed on the 3D coordinate work table, and four cameras are connected with external trigger signals, which control the four cameras to collect rail images synchronously to ensure the accuracy of the analysis of image matching points. Taking a certain position of the three-dimensional coordinate table as the starting point, the change value of the distance between the two rails is adjusted, and the calculation is carried out by the algorithm introduced above. The test results of gauge change are shown in Table 1.

**Table 1.** Gauge change detection test results

| Number | Offset value/mm | Measurement value/mm | Error value/mm |
|---|---|---|---|
| 1 | -5.00 | -5.017 | -0.017 |
| 2 | -3.00 | -3.041 | -0.041 |
| 3 | -2.50 | -2.518 | -0.018 |
| 4 | -2.00 | -2.001 | -0.001 |
| 5 | -1.50 | -1.495 | 0.005 |
| 6 | ł1.00 | ł0.996 | 0.004 |
| 7 | ł0.80 | ł0.833 | ł0.033 |
| 8 | ł0.60 | ł0.628 | ł0.028 |
| 9 | ł0.40 | ł0.429 | ł0.029 |
| 10 | ł0.20 | ł0.176 | 0.024 |
| 11 | 0.20 | 0.226 | 0.026 |
| 12 | 0.40 | 0.441 | 0.041 |
| 13 | 0.60 | 0.626 | 0.026 |
| 14 | 0.80 | 0.868 | 0.068 |
| 15 | 1.00 | 1.045 | 0.045 |
| 16 | 1.50 | 1.528 | 0.028 |
| 17 | 2.00 | 2.049 | 0.049 |
| 18 | 2.50 | 2.532 | 0.032 |
| 19 | 3.00 | 2.958 | ł0.042 |
| 20 | 5.00 | 5.041 | 0.041 |

It can be seen from Table 1 that the detection system can effectively detect the variation value of the gauge, and the maximum error is 0.068mm, and the relative error decreases with the increase of the variation value of the gauge.

The gauge detection system designed based on the machine vision method will be installed in the axle box accessories of the vehicle. The vehicle will inevitably vibrate in the actual running process, and the gauge detection system will also vibrate along with the axle box. Therefore, it is necessary to verify the ability of the system to capture gauge points. The rail is placed on the three-dimensional coordinate platform, a certain point is set as the starting point, the upper and lower height of the rail is adjusted, and the space coordinate of the gauge point is calculated using binocular vision (only for unilateral track), and the distance between the space coordinate point and the starting point is calculated, and the test data in Table 2 is obtained. It can be seen from Table 2 that most of the errors are within 0.1mm, only some are above 0.1mm, and the maximum error is 0.158mm. This error has little effect on gauge measurement. The test results show that the system has good robustness and the detection results are not affected by vibration. The above experimental process was repeated in the laboratory, and the results obtained were basically consistent. The results have good repeatability.

**Table 2.** Gauge points capture test results

| Number | Offset value/mm | Measurement value/mm | Error value/mm |
|---|---|---|---|
| 1 | ł20.00 | ł20.158 | ł0.158 |
| 2 | ł15.00 | ł14.998 | 0.002 |
| 3 | ł10.00 | ł10.019 | ł0.019 |
| 4 | ł5.00 | ł5.001 | ł0.001 |
| 5 | ł3.00 | ł2.999 | 0.001 |
| 6 | ł2.00 | ł1.909 | 0.091 |
| 7 | ł1.00 | ł1.068 | ł0.068 |
| 8 | 1.00 | 0.943 | ł0.057 |
| 9 | 2.00 | 1.986 | ł0.014 |
| 10 | 3.00 | 2.929 | ł0.071 |
| 11 | 5.00 | 4.963 | ł0.037 |
| 12 | 0.00 | 9.950 | ł0.050 |
| 13 | 15.00 | 14.890 | ł0.110 |
| 14 | 20.00 | 19.987 | ł0.013 |

## 6. Conclusion

It is of great practical significance to study the intelligent gauge detection system for urban rail transit and high-speed railway. The intelligent gauge detection system can reflect the track status in time, which plays an important role in warning the safety of train operation and reducing the manpower and financial resources of track maintenance. The gauge detection system based on machine vision has the characteristics of high precision and strong anti-interference ability. The maximum tracking error of gauge point is only 0.158mm, and the measurement accuracy reaches 0.07mm, which improves the speed, accuracy and reliability of gauge detection, and can meet the requirements of high-precision dynamic gauge detection.

## 7. Conflict of Interest

The authors declare that there are no conflict of interests, we do not have any possible conflicts of interest.

**Acknowledgments.**

This paper was supported by the Research Project of Zhengzhou University of Science and Technology: Vibration Analysis and Control Based on Flexible Joints and Loads of Industrial Robots (2022XJKY05); 2023 Teacher Development Research Project of Zhengzhou University of Science and Technology, Research on Career Development Dilemma and Implementation Path of Young Teachers in Application-oriented Universities in the New Era (JSFZZXKT2023004); Key Research Project of Universities in Henan Province "Development and Research of Intelligent Gauge Detection System of Rail Transit Based on Dynamic Distance Measurement" (24B460027).

## References

1. Li Z, Zhao J, Peng Q. Train service design in an urban rail transit line incorporating multiple service routes and multiple train compositions[J]. Transportation Research Part C: Emerging Technologies, 2021, 123: 102959.
2. Zhou Y, Yang H, Wang Y, et al. Integrated line configuration and frequency determination with passenger path assignment in urban rail transit networks[J]. Transportation Research Part B: Methodological, 2021, 145: 134-151.
3. Yin S, Li H, Laghari A A, et al. FLSN-MVO: Edge Computing and Privacy Protection Based on Federated Learning Siamese Network With Multi-Verse Optimization Algorithm for Industry 5.0[J]. IEEE Open Journal of the Communications Society, 2024.
4. Hou B, Cao Y, Lv D, et al. Transit-based evacuation for urban rail transit line emergency[J]. Sustainability, 2020, 12(9): 3919.
5. Yang A, Wang B, Huang J, et al. Service replanning in urban rail transit networks: Cross-line express trains for reducing the number of passenger transfers and travel time[J]. Transportation Research Part C: Emerging Technologies, 2020, 115: 102629.
6. Yin, S., Wang, L., Teng, L. Threshold Segmentation Based on Information Fusion for Object Shadow Detection in Remote Sensing Images. Computer Science and Information Systems, vol. 21, no. 4, 1221-1241. (2024). https://doi.org/10.2298/CSIS231230023Y.
7. S. Yin, H. Li, Y. Sun, M. Ibrar, and L. Teng. Data Visualization Analysis Based on Explainable Artificial Intelligence: A Survey[J].?IJLAI Transactions on Science and Engineering, vol. 2, no. 2, pp. 13-20, 2024.
8. Shoulin Yin, Hang Li, Asif Ali Laghari, Thippa Reddy Gadekallu, et al. An Anomaly Detection Model Based on Deep Auto-encoder and Capsule Graph Convolution via Sparrow Search Algorithm in 6G Internet-of-Everything[J]. IEEE Internet of Things Journal, vol. 11, no. 18, pp. 29402-29411, 2024. DOI: 10.1109/JIOT.2024.3353337.
9. Li H, Zhao C. Fusion Cycle GAN: A Multiple Feature Fusion based Cycle-consistent Generative Adversarial Network for Person Re-Identification[J]. Journal of Science and Engineering, 2024, 1(1): 7-12.
10. Ibrar M, Sun Y. SEIR Model Based Epidemic Transmission Risk Deep Prediction[J]. Journal of Science and Engineering, 2024, 1(1): 25-31.
11. Zhang M, Qin C, Qiang F. Leveraging Artificial Intelligence to Assess Physicians Willingness to Share Electronic Medical Records in a Hierarchical Diagnostic Ecosystem[J]. Journal of Artificial Intelligence Research, 2024, 1(1): 55-72.
12. Liu W. Channel Reorganization for Few-Shot Segmentation[J]. Journal of Artificial Intelligence Research, 2024, 1(1): 73-82.
13. Pan D, Zhao L, Luo Q, et al. Study on the performance improvement of urban rail transit system[J]. Energy, 2018, 161: 1154-1171.
14. Du Q, Huang Y, Zhou Y, et al. Impacts of a new urban rail transit line and its interactions with land use on the ridership of existing stations[J]. Cities, 2023, 141: 104506.
15. Wang L, Shoulin Y, Alyami H, et al. A novel deep learning-based single shot multibox detector model for object detection in optical remote sensing images [J]. Geoscience Data Journal, vol. 11, no. 3, pp. 237-251, 2024. SCI IF=3.488, https://doi.org/10.1002/gdj3.162.
16. Teng L. Brief Review of Medical Image Segmentation Based on Deep Learning[J]. IJLAI Transactions on Science and Engineering, 2023, 1(02): 01-08.

17. Jiang, Y., Yin, S. Heterogenous-view Occluded Expression Data Recognition Based on Cycle-Consistent Adversarial Network and K-SVD Dictionary Learning Under Intelligent Cooperative Robot Environment[J]. Computer Science and Information Systems, vol. 20, no. 4, 2023.
18. Mohebbian M R, Marateb H R, Wahid K A. Semi-supervised active transfer learning for fetal ECG arrhythmia detection[J]. Computer Methods and Programs in Biomedicine Update, 2023, 3: 100096.
19. Hurley-Walker N, Rea N, McSweeney S J, et al. A long-period radio transient active for three decades[J]. Nature, 2023, 619(7970): 487-490.
20. Yin S, Wang L, Wang Q, et al. M2F2-RCNN: Multi-functional faster RCNN based on multi-scale feature fusion for region search in remote sensing images[J]. Computer Science and Information Systems, vol. 20, no. 4, 2023.
21. Yin S, Wang L, Shafiq M, et al. G2Grad-CAMRL: an object detection and interpretation model based on gradient-weighted class activation map** and reinforcement learning in remote sensing images[J]. IEEE Journal of Selected Topics in Applied Earth Observations and Remote Sensing, 2023, 16: 3583-3598.
22. Teng L, Qiao Y, Shafiq M, et al. FLPK-BiSeNet: Federated learning based on priori knowledge and bilateral segmentation network for image edge extraction[J]. IEEE Transactions on Network and Service Management, 2023, 20(2): 1529-1542.
23. Jisi A?and Shoulin Yin. A New Feature Fusion Network for Student Behavior Recognition in Education [J]. Journal of Applied Science and Engineering. vol. 24, no. 2, pp.133-140, 2021.
24. Yu J, Zhao L. A novel deep CNN method based on aesthetic rule for user preferential images recommendation[J]. Journal of Applied Science and Engineering, 2021, 24(1): 49-55.
25. S. Yin and H. Li. Hot Region Selection Based on Selective Search and Modified Fuzzy C-Means in Remote Sensing Images[J]. IEEE Journal of Selected Topics in Applied Earth Observations and Remote Sensing, vol. 13, pp. 5862-5871, 2020, doi: 10.1109/JSTARS.2020.3025582.

## Biography

**Jiyue Wang** is with the School of Vehicle and Traffic Engineering, Zhengzhou University of Science and Technology, Zhengzhou 450064 China. Research direction: Image processing, data analysis, artificial intelligence.